frontiers in Physics

ORIGINAL RESEARCH
published: 08 December 2021
doi: 10.3389/fphy.2021.711212

Polarization-Singular Approach to Imaging Mueller-Matrix Polarimetry in the Differential Diagnosis of Histological Sections of Biopsy of Tumors of the Uterus and Prostate

A. Dubolazov[1], V. Ushenko[1], L. Trifonyuk[2], A. Stashkevich[3], I. Soltys[1], Y. Ushenko[1], Y. Tomka[1], A. Ushenko[1,4], V. Gantyuk[1] and P. Gorodensky[1]*

[1]Chernivtsi National University, Chernivtsi, Ukraine, [2]Rivne Regional Clinical Hopital, Rivne, Ukraine, [3]Institute of Traumathology and Orthopedics of NAMS, Kyiv, Ukraine, [4]Research Institute of Zhejiang University, Taizhou, China

OPEN ACCESS

Edited by:
Steen Grüner Hanson,
Technical University of Denmark,
Denmark

Reviewed by:
Sébastien Robert Mouchet,
University of Exeter, United Kingdom
Nirmal Mazumder,
Manipal Academy of Higher
Education, India

***Correspondence:**
A. Dubolazov
a.dubolazov@chnu.edu.ua

Specialty section:
This article was submitted to
Optics and Photonics,
a section of the journal
Frontiers in Physics

Received: 18 May 2021
Accepted: 07 October 2021
Published: 08 December 2021

Citation:
Dubolazov A, Ushenko V, Trifonyuk L, Stashkevich A, Soltys I, Ushenko Y, Tomka Y, Ushenko A, Gantyuk V and Gorodensky P (2021) Polarization-Singular Approach to Imaging Mueller-Matrix Polarimetry in the Differential Diagnosis of Histological Sections of Biopsy of Tumors of the Uterus and Prostate.
Front. Phys. 9:711212.
doi: 10.3389/fphy.2021.711212

The possibilities of the diagnostic use of the singular approach of the distributions of the number of characteristic values of the MMI is effective for differentiating the polarization properties of histological biopsy sections of benign and malignant tumours of the uterus and prostate. Within the framework of evidence-based medicine, the sensitivity, specificity and accuracy of the azimuthal-invariant express (~15 min) method of Mueller-matrix mapping of polarization-singular states in the differential diagnosis of uterine myoma and adenocarcinoma, as well as adenocarcinoma of the prostate with varying degrees of differentiation have been determined.

Keywords: mueller matrix, singularity, polarization, S and C-state, optical anisotropy, birefringence, biological tissue, statistical moments

INTRODUCTION

In biomedical optics, polarized light plays a decisive role in understanding and detecting the processes of conversion of electromagnetic waves by optically anisotropic structures of human biological tissues [1–20]. The most important analytical direction in the development of diagnostic techniques using polarization probing of biological layers is the Mueller-matrix formalism [10]. This approach provides the most complete information on the optical anisotropy of diagnostic objects. Several key strands of investigation have emerged, including: Mueller matrix polarimetry (MMP) [21–24] polar decomposition of Mueller matrices [25, 26]; and two [27–32] dimensional Mueller matrix mapping (MMM) using various approximations [19, 20, 33].

One of the main tasks of MMP is to detect and differentiate the type of oncological changes that occur in the tissues of human organs. Using MMM methods [14–16, 23–26], the possibility of differential diagnosis of histological sections of biopsy of benign and malignant tumours of the prostate, endometrium, cervix, breast, etc. has been demonstrated. However, the further successful development of MMP restrains a number of theoretical and experimental problems that have not been resolved to the end:

- Azimuthal dependence of the value of 12 out of 16 elements of the Mueller matrix, which worsens the accuracy of MMM methods in the process of serial measurements of histological preparations;

- ❖ Significant "computational" time required for processing large arrays of experimental data obtained by polar decomposition of Mueller matrices and two-dimensional MMM;
- ❖ Distorting effect of the depolarized background on the Mueller-matrix detection of optical anisotropy of tissue samples of human organs [34].

One of the options for a comprehensive solution to these MMP problems can be the synthesis of MMM methods of optically thin (non-depolarizing) biological preparations and the principles of polarization-singular analysis of their object fields [1–5, 7, 9]. The main idea of this approach is that for such layers there are direct relationships between the points of linear ("*L*") and circular ("*C*") polarization states of the microscopic image and the characteristic values of azimuthally invariant matrix elements that characterize the optical anisotropy of fibrillar networks.

At this point in time in biomedical optics, singular approaches were applied in so far, few publications [35–37]. Here, for the first time, the analytical conditions for the formation of singly (linear) and doubly degenerate (circular) polarization singularities of images of linearly birefringent biological tissues are determined. The distributions of the number of polarization singular states in the images of such biological tissues are experimentally investigated. It has been demonstrated that the statistical moments, which characterize the distributions of the number of singular points in the object field, are sensitive to changes in morphological structure of biological tissues of various physiological state.

However, this direction of biomedical diagnostics remains poorly researched and requires further extension of the ideology of the singularity of optical fields to methods and means of one of the most effective optical technologies–azimuthally invariant MMP of the polycrystalline component of pathologically altered tissues of various human organs.

Our work is aimed at:

- ❖ Identification of analytical relationships between polarization-singular states of the object field of optically thin anisotropic layers of tissues of the uterus and prostate and characteristic values of their Mueller-matrix images;
- ❖ Development of a new azimuthally invariant Mueller-matrix polarization-singular technique for serial and express (~15 min) measurements for differential diagnosis of changes in optical anisotropy caused by tumours of uterus (malignant myoma and malignant adenocarcinoma) and prostate (adenocarcinoma with different malignant grades) tissues.

The relevance of such studies is associated with the widespread prevalence and high mortality caused by these cancers.

Prostate cancer is the second most common cancer globally in men, and in some countries is now the most diagnosed form of cancer [38, 39]. Early diagnosis, intervention, and management can give significantly improved patient outcomes [40]. It is necessary to differentiate between malignant (carcinoma) grades of tumour tissues [41]. A similar situation is realized for uterine cancer, which ranks fourth among women oncological diseases [42].

BRIEF THEORY AND BASIC RELATIONS

In a polarization-inhomogeneous field, the existence of lines or surfaces is possible, at each point of which an indefinite (singular) one of its parameters [1–5, 7, 9]:

1) points of circular polarization of the field ("C"-point), in which the polarization ellipse degenerates into a circle and, accordingly, the direction of the main axis (azimuth) of the polarization ellipse is uncertain;
2) points with linear polarization ("L"-point), which are degenerate in the direction of rotation of the electric vector.

The characteristic values of the fourth parameter VS_4 of the Stokes vector VS are used as the main "detector" of the presence and coordinate position of polarization-singular points in the object field of laser radiation [6, 8, 10].

$$VS_4(r) = 0 \Leftrightarrow L(\phi = k\pi), k = 0; 1; 2; \ldots; \quad (1)$$

$$VS_4(r) = \pm 1 \Leftrightarrow \pm C(\phi = 0.5(2k+1)\pi) \quad (2)$$

Here r—spatial coordinate in a polarization-inhomogeneous object field; ϕ—phase shift between orthogonal amplitude components at a point r.

At the same time, the analytical representation of the grid of polarization singularities of the object field of laser radiation does not carry direct information about the polycrystalline structure of the biological layer—the distributions of the directions of the optical axes $\chi(r)$ of biological crystals and the phase shifts $\varphi(r)$ that they form.

The fact is that the process of formation of a polarization-inhomogeneous field can be represented by a superposition of two main mechanisms:

- ❖ "object"-phase modulation $[\varphi(r)]$ of probing laser radiation with optically anisotropic birefringent biological crystals (protein fibrillar networks);
- ❖ "diffractive"—secondary phase modulation $[\varphi(r) = \varphi(r) + \delta(r)]$ as a result of cross-interference of partial laser waves formed by an object of a polarization-inhomogeneous object field during propagation in free space.

Therefore, in each zone of laser radiation diffraction, the maps of polarization singularities $[L(r)$ and $C(r)]$ change. As a result, the problem of polarimetric diagnostics of changes in the structure of the biological layer turns out to be ambiguous.

Overcoming this problem can be the use of the Mueller-matrix formalism [10] in the description of the processes of the formation of the polarization-singular structure of the object field of an optically anisotropic biological layer. This approach

provides unambiguous information on the relationships between the maps of polarization singularities and the parameters of the polycrystalline birefringent structure of fibrillar networks.

$$\begin{array}{l} \mathrm{L}(\mathrm{r}) \Leftrightarrow \mathrm{w}(\chi, \varphi); \\ \mathrm{C}(\mathrm{r}) \Leftrightarrow \mathrm{v}(\chi, \varphi). \end{array} \tag{3}$$

Within the framework of the model of birefringence of spatially structured fibrillar networks of the biological layer, developed in numerous studies [12–16, 18, 27–32], one can write the following expression for the Mueller matrix

$$\{\mathrm{F}\}(\mathrm{r}) = \begin{Vmatrix} 1 & 0 & 0 & 0 \\ 0 & f_{22} & f_{23} & f_{24} \\ 0 & f_{32} & f_{33} & f_{34} \\ 0 & f_{42} & f_{43} & f_{44} \end{Vmatrix}(\mathrm{r}), \tag{4}$$

where

$$\mathrm{f_{ik}} = \begin{cases} \mathrm{f_{22}} = \cos^2 2\chi + \sin^2 2\chi \cos\varphi, \\ \mathrm{f_{23}} = \mathrm{f_{32}} = \cos 2\chi \sin 2\chi (1 - \cos\varphi), \\ \mathrm{f_{33}} = \sin^2 2\chi + \cos^2 2\chi \cos\varphi, \\ \mathrm{f_{42}} = -\mathrm{f_{24}} = \sin 2\chi \sin\varphi, \\ \mathrm{f_{34}} = -\mathrm{f_{43}} = \cos 2\chi \sin\varphi, \\ \mathrm{f_{44}} = \cos\varphi. \end{cases} \tag{5}$$

Here χ—direction of the optical axis, determined by the orientation of the position of the fibril in the plane of the biological layer; $\varphi = 2\pi/\lambda \Delta \mathrm{nz}$—object phase shift between linearly orthogonally polarized components of the laser beam amplitude; $\boldsymbol{\lambda}$—wavelength; $\Delta\mathbf{n}$—birefringence; z—geometric layer thickness.

The Mueller-matrix formalism for describing the birefringent properties of biological tissues makes it possible to exhaustively describe the formation of polarization at the points (r) of the object field in terms of the parameters of the Stokes' vector VS [10].

$$\mathrm{VS}^*(r) = \|\mathrm{F}\|(\mathrm{r})\mathrm{VS}^0(\mathrm{r}) \tag{6}$$

Here$\mathrm{VS}^0(\mathrm{r})$ и $\mathrm{VS}^*(\mathrm{r})$—Stokes' vectors of probing and transformed by a layer of biological tissue of laser beams.

In expanded form, matrix **Eq. 6** is rewritten as a system of four linear equations with coefficients f_{ik}

$$\begin{cases} \mathrm{VS}_1^*(\mathrm{r}) = \mathrm{VS}_1^0(\mathrm{r}); \\ \mathrm{VS}_2^*(\mathrm{r},\rho,\delta) = \mathrm{f_{22}}(\mathrm{r},\rho,\delta)\mathrm{VS}_2^0 + \mathrm{f_{23}}(\mathrm{r},\rho,\delta)\mathrm{VS}_3^0 + \mathrm{f_{24}}(\mathrm{r},\rho,\delta)\mathrm{VS}_4^0; \\ \mathrm{VS}_3^*(\mathrm{r},\rho,\delta) = \mathrm{f_{32}}(\mathrm{r},\rho,\delta)\mathrm{VS}_2^0 + \mathrm{f_{33}}(\mathrm{r},\rho,\delta)\mathrm{VS}_3^0 + \mathrm{f_{34}}(\mathrm{r},\rho,\delta)\mathrm{VS}_4^0; \\ \mathrm{VS}_4^*(\mathrm{r},\rho,\delta) = \mathrm{f_{42}}(\mathrm{r},\rho,\delta)\mathrm{VS}_2^0 + \mathrm{f_{43}}(\mathrm{r},\rho,\delta)\mathrm{VS}_3^0 + \mathrm{f_{44}}(\mathrm{r},\rho,\delta)\mathrm{VS}_4^0; \end{cases} \tag{7}$$

Taking into account relations **Eqs 4**–, expressions **Eq. 3**, which characterize the Stokes-polarimetric relationships **Eqs 1**, **2** of maps of polarization singularities and parameters of the polycrystalline birefringent structure of fibrillar networks, take the following form

$$\begin{array}{l} \mathrm{VS_4}(\mathrm{r},\pm\mathrm{C}) = \pm\sin 2\rho(\mathrm{r})\mathrm{VS}_2^0 \pm \cos 2\rho(\mathrm{r})\mathrm{VS}_3^0; \\ \mathrm{VS_4}(\mathrm{r},\mathrm{L}) = \cos 4\rho(\mathrm{r})\mathrm{VS}_2^0 + \sin 4\rho(\mathrm{r})\mathrm{VS}_3^0. \end{array} \tag{9}$$

Analysis of expressions **Eq. 9** reveals two main dependences of formation L and C states:

❖ "polarizing"

$$\begin{array}{l} \mathrm{VS_4}(\mathrm{r},\pm\mathrm{C}) \Leftrightarrow \mathrm{VS}_2^0; \mathrm{VS}_3^0; \\ \mathrm{VS_4}(\mathrm{r},\mathrm{L}) \Leftrightarrow \mathrm{VS}_2^0; \mathrm{VS}_3^0. \end{array} \tag{10}$$

❖ "azimuth"

$$\begin{array}{l} \mathrm{VS_4}(\mathrm{r},\pm\mathrm{C}) \Leftrightarrow \sin 2\rho(\mathrm{r});\ \cos 2\rho(\mathrm{r}); \\ \mathrm{VS_4}(\mathrm{r},\mathrm{L}) \Leftrightarrow \cos 4\rho(\mathrm{r});\ \sin 4\rho(\mathrm{r}). \end{array} \tag{11}$$

Hence (expressions **Eqs 10**, **11**) there are significant limitations in the use of the Stokes-parametric approach in diagnostic serial measurements of maps of polarization singularities of a large number of biological preparations. Even in the situation of a constant polarization state ($(\mathrm{VS}_2^0; \mathrm{VS}_3^0) = \mathrm{const}$) of the probing laser beam, the coordinate position of the $L(r;\chi)$ and $C(r;\chi)$ - points turns out to be dependent on the angle of rotation (Ψ) of the biological preparation - $L(r_1;\chi \pm \Psi)$ and $C(r_1;\chi \pm \Psi)$. The indicated azimuthal irreproducibility of polarization-singular data is multiplied within the limits of representative samplings of biological samples.

To overcome this problem of Stokes polarimetry, we considered the diagnostic capabilities of the polarization-singular approach using the Mueller-matrix formalism.

Based on relations **Eqs 3**–**5**, it is possible to determine diagnostically important relationships between the characteristic values of the elements of the Mueller matrix of the conditions of formation $L(r;\chi)$ and $C(r;\chi)$ polarization-singular states that are formed by a birefringent fibrillar network—**Table 1**.

The analysis of the ratios given in **Table 1** revealed an azimuthal dependence of the formation of characteristic values $\begin{pmatrix} \mathrm{f_{ik}}(\mathrm{r},\chi) \Leftrightarrow \mathrm{q}(\mathrm{L}); \\ \mathrm{f_{ik}}(\mathrm{r},\chi) \Leftrightarrow \mathrm{g}(\pm\mathrm{C}) \end{pmatrix}$ of practically all elements of the Mueller matrix of the birefringent biological layer. The exception (highlighted in green) is the matrix element f_{44}, which in what follows we will call the Mueller-matrix invariant–MMI.

Measurement and Analysis of Experimental Data

In **Figure 1** shows the optical scheme of Stokes polarimetry [14, 15] of the coordinate distributions of the Mueller-matrix invariant f_{44}, which characterizes the birefringence of histological sections of uterine tumours.

The optical and metrological parameters of the Stokes-polarimeter are presented in detail in a series of publications [14, 15, 27–32]. Here we give a brief description of them, which is necessary for a better understanding of the further presentation of the experimental material.

Illumination of samples was performed by parallel ($\boldsymbol{\text{Ø}} = 2 \times 10^3 \mu\mathrm{m}$) weakly intensive ($\mathrm{p} = 5\,\mathrm{mW}$) beam 1 of He-

TABLE 1 | Relationships between the characteristic values of the Mueller matrix elements and the singularity of polarization-inhomogeneous images of birefringent biological tissue.

f_{ik}	"L"-point ($\phi = 0$, $\phi = \pi$)	"+C"- point ($\phi = +\pi/2$)	"−C"-point ($\phi = -\pi/2$)
f_{22}	1; $\cos 4\chi$	$\cos^2 2\chi$	$\cos^2 2\chi$
$f_{23} = f_{32}$	0; $\sin 4\chi$	$0.5 \sin 4\chi$	$0.5 \sin 4\chi$
$f_{24} = -f_{42}$	0	$\sin 2\chi$	$-\sin 2\chi$
f_{33}	1; $\cos 4\chi$	$\sin^2 2\chi$	$\sin^2 2\chi$
$f_{34} = -f_{43}$	0	$\cos 2\chi$	$-\cos 2\chi$
f_{44}	±1	0	0

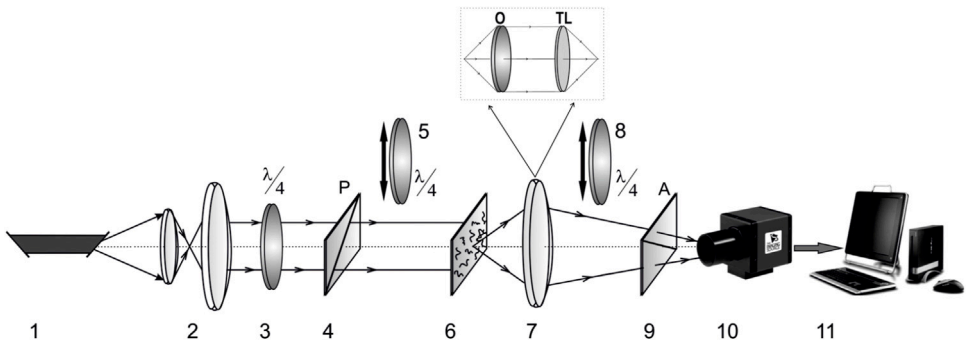

FIGURE 1 | Optical scheme of laser Stokes-polarimeter of human organs histological sections. Here 1—He-Ne laser; 2—collimator; 3, 5, 8—quarter-wave plates; 4, 9—polarizer and analyzer respectively; 6—object of investigation; 7—optical system; 10—CCD camera; 11—PC.

Ne laser (λ = 0.6328μm). Using a collimated illuminating beam provides the same conditions of transformation of the polarization states at different points of the illuminated area of the object. In this case, our scheme provides the resolution of 4.65 × 4.65 μm. This scale is sufficient to evaluate the optical properties of the average (5–20 μm) crystalline structural elements of the biological samples. Polarization light source consisted of quarterwave plate 3 and polarizer 4. The image of samples 6 were projected in the plane of light-sensitive plane of CCD-camera 10 (The Imaging Source DMK 41AU02. AS, monochrome 1/2″ CCD, Sony ICX205AL (progressive scan); resolution—1280 × 960; size of light-sensitive plate—5952 × 4464 μm; sensitivity—0.05 lx; dynamic range—8 bit; SNR—9 bit, nonlinearity does not exceed 3–5%) by means of optical system 7. In this experimental arrangement 7 designates an image forming apparatus, which consists of strain-free objective (Nikon CFI Achromat P, working distance—30 mm, focal distance—50mm, NA—0.1, magnification—4x) and tube lens (focal distance 200 mm). Polarization analysis of the samples images was performed by means of quarterwave plate 8 and polarizer-analyzer 9.

The technique of experimental measurement of the set of characteristic elements of the Mueller-matrix invariant f_{44} includes the following actions:

1) Formation of the basic right-hand circularly polarized probing beam—the angle between the plane of polarization of the laser beam and the axis of the highest velocity of the quarter-wave plate—Θ = +45°.
2) Isolation by sequential polarization filtering of a set of partial plane and circularly polarized laser probes with the following parameters:
   - ❖ azimuth of linear polarization A = 0°—rotation of the transmission plane of polarizer 4 by an angle Θ = 0°;
   - ❖ azimuth of linear polarization A = 90°—rotation of the transmission plane of polarizer 4 by an angle Θ = 90°;
   - ❖ introduction of a quarter-wave plate 5 into the optical path and rotation of the axis of its highest velocity by an angle Θ = +45°.
3) Projection by a polarizing microobjective 7 for each of the laser probes of the image of a histological section of a preparation of a uterine tumour into the plane of the photosensitive area of a digital camera 10.
4) Polarization selection of the right- and left-circularly polarized components of the object field at the points of the microscopic image by rotating the axis of the highest velocity of the quarter-wave plate 8 at angles Θ = +45° and Θ = −45° relative to the transmission plane of the polarizer 9.
5) Calculations within each pixel of CCD camera 10 of the ensemble (m × n) of the Muller-matrix invariant quantities of f_{44} elements of the biological layer sample were performed in accordance with the algorithm

$$f_{44}(m \times n) = VS_4^{\otimes}(m \times n) - 0.5\left(VS_4^{0}(m \times n) + VS_4^{90}(m \times n)\right). \quad (12)$$

Here $VS_{i=4}^{0;90;\otimes}$—Stokes vector parameter of the points of the digital image (m × n) of a biological layer sample measured for a series of linear (0° ; 90°) and right-circularly (⊗) polarized laser beams

$$VS_{i=4}^{0;90;\otimes}(m \times n) = I_{\otimes}^{0;90;\otimes}(m \times n) + I_{\oplus}^{0;90;\otimes}(m \times n). \quad (13)$$

Here $I_{\otimes;\oplus}$—the intensity of transmitted by the object light that passed through a system of "quarter-wave plate–polarizer" of polarization analysis unit which transmits right- (⊗) and left- (⊕) circularly polarized components of the object laser radiation.

6) The accuracy of determining the value $f_{44}(m \times n)$ is 2% and was determined through a series of measurements using model phase-shifting plates ″0.25λ″ and ″0.5λ″.
7) By line-by-line scanning ($n_{i+1} = n_i + 1$pix) was determined (within each column $m_i \div m_i + 1$pix) the number of characteristic values $f_{44} = 0 \Leftrightarrow (\pm C)$ and $f_{44} = \pm 1 \Leftrightarrow (L)$. On this basis, the distributions of the number of characteristic values $N(f_{44} = 0)$ and $M(f_{44} = \pm 1)$ were finding.
8) We calculated [14, 15, 42] the central statistical moments of the first–second orders, which characterize the average and dispersion of the distribution $N(f_{44} = 0)$ and $M(f_{44} = \pm 1)$

$$\begin{cases} Z_1 = \dfrac{1}{W}\sum_{j=1}^{W}\left(\left(N(f_{44}=0)\right)(m \times n)\right)_j; \\ Z_2 = \sqrt{\dfrac{1}{W}\sum_{j=1}^{W}\left(\left(N^2(f_{44}=0)\right)(m \times n)\right)_j}; \\ Z_1 = \dfrac{1}{W}\sum_{j=1}^{W}\left(\left(M(f_{44}=\pm 1)\right)(m \times n)\right)_j; \\ Z_2 = \sqrt{\dfrac{1}{W}\sum_{j=1}^{W}\left(\left(M^2(f_{44}=0)\right)(m \times n)\right)_j}. \end{cases} \quad (13)$$

Here W = m × n—total number of pixels of a digital camera 10 (**Figure 1**).

Characteristics of Research Objects

For the purpose of express (~15 min) differential diagnosis of benign (myoma) and malignant (adenocarcinoma of varying degrees of differentiation), optically thin single-scattering histological sections of uterine tumours were made on a microtome with rapid freezing during the operation.

Three representative groups of histological biopsy sections of tumours were formed:

- Group 1 consisted of n = 40 myoma samples;
- Group 2 consisted of n = 36 high differentiated adenocarcinoma samples;
- Group 3 consisted of n = 36 poorly differentiated adenocarcinoma samples.

The type of uterus tumour was determined by an independent assessment of stained histological samples (**Figure 2**).

- ❖ Fixation of prostate tissue with formalin (40% formaldehyde aqueous solution);
- ❖ Washing samples in running water for 24 h;
- ❖ Dehydration with alcohols with increasing concentration (70–100%) within 48 h;
- ❖ Fixing the material in a mixture of xylene-paraffin for 1–2 h at a temperature of $52^{\circ}C - 56^{\circ}C$ and cutting out a block with a sample enclosed in it;
- ❖ Production of histological sections on a standard microtome;
- ❖ Staining of histological sections with hematoxylin-eosin (**Figure 2** shows microscopic images in real colors);
- ❖ Microscopic examination of images of the obtained preparations with differentiation of their structure by grade and determination of the position of the prostate tumor sample according to the Gleason scale.

Table 2 presents the optical and geometric parameters of the samples of native histological sections of prostate tumour biopsies from each of the groups.

The geometric thickness (z, μm) of histological sections of prostate tissue was determined by the standard values of the freezing microtome scale.

The extinction coefficient (τ, cm^{-1}) of uterus tissue samples was measured according to the standard method of photometric measurement of the attenuation by the sample of the intensity of the illuminating beam [44] using an integral light scattering sphere [45].

The measurement of the integral degree of depolarization (Λ, %) of samples of histological sections of uterus tissue was carried out in the scheme of a standard Mueller-matrix polarimeter, the optical scheme of which is presented in [14, 15, 27–32].

The experimental data presented in **Table 2** indicate the adequacy of our model analysis of the phase modulation of laser radiation by birefringent fibrillar networks (relations **Eqs 4–11**, **Table 1**)—within the statistically reliable samplings of samples of all groups, the conditions of single scattering are realized ($\tau \le 0.1; \Lambda \to 0$ [16]) in the volume of histological sections of biopsy of uterine tumours.

To determine the statistical significance of a representative sampling of the number of samples by the cross-validation method [46], the standard deviation θ^2 of each of the calculated values of the central statistical moments $Z_{i=1;2}(n)$, which characterize the distribution of the values of parameters of $N(f_{44} = 0)$ and $M(f_{44} = \pm 1)$, was determined. The specified number (40 for each group) of samples provided the level $\theta^2 \le 0.025$. This standard deviation corresponds to a confidence interval $p < 0.05$, which demonstrates the statistical reliability of the polarization-interference mapping method.

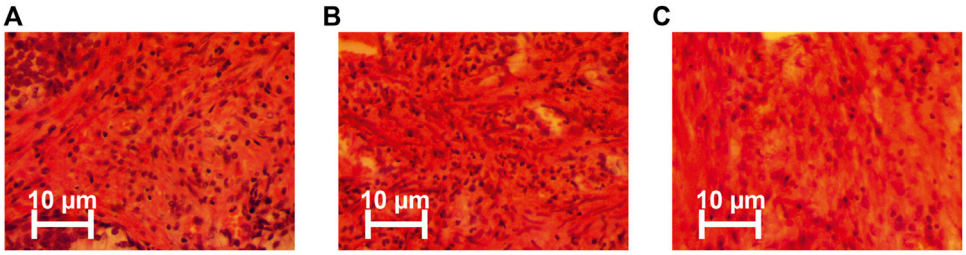

FIGURE 2 | Representative microscopic images (magnification 50x) of: **(A)** myoma, **(B)** high differentiated adenocarcinoma, and **(C)** poorly differentiated uterus adenocarcinoma. The procedure for histological analysis included the following steps [43].

TABLE 2 | Optical and geometric parameters of uterus tumour histological sections.

Parameters	Group 1	Group 2	Group 3
Geometric thickness $h, \mu m$	15 ± 0.07	15 ± 0.065	15 ± 0.07
Attenuation (extinction) coefficient τ, cm^{-1}	0.098 ± 0.0041	0.097 ± 0.0037	0.101 ± 0.0049
Depolarization degree $\Lambda, \%$	3 ± 0.18	3 ± 0.17	4 ± 0.19

RESULTS

In the series in **Figures 3–5** are presented:

- Coordinate distributions of the value of the Mueller-matrix invariant $f_{44}(m \times n)$ of histological biopsy sections of benign (**Figure 3**) and malignant with varying degrees of differentiation (**Figure 4** and **Figure 5**) of uterine tumours [fragments (2)];
- Maps of characteristic values $(f_{44} = \pm 1)(m \times n)$ [fragments (3)];
- Maps of characteristic values $(f_{44} = 0)(m \times n)$ [fragments (3)].
- Analysis of 2D mapping data (**Figures 3–5**) the values of the Mueller-matrix invariant $f_{44}(m \times n)$ in the plane of histological sections of biopsy of all types of tumours revealed:
- The presence of characteristic values $(f_{44} = \pm 1)(m \times n)$ [fragments (1)] and $(f_{44} = 0)(m \times n)$ [fragments (3)] with individual coordinate and quantitative distribution;
- sequential increase in the number of characteristic values $(f_{44} = \pm 1)(m \times n)$ for samples of malignant tumours of adenocarcinoma with high [**Figure 4**, fragment (1)] and low [**Figure 5**, fragment (1)] degrees of differentiation in comparison with benign myoma [**Figure 3**, fragment (1)];
- the opposite trend for maps $(f_{44} = 0)(m \times n)$—a sequential decrease in the number of characteristic values for malignant tumour samples of adenocarcinoma with a high [**Figure 4**, fragment (3)] and low [**Figure 5**, fragment (3)] degrees of differentiation in comparison with benign myoma [**Figure 3**, fragment (3)].

From a physical point of view, these results can be associated with the processes of necrotic destruction of birefringent fibrillar networks of the uterine tissue during the formation of benign neoplasms (myoma) of malignant adenocarcinomas with varying degrees of differentiation. As a result, the level of phase modulation $(\phi(m \times n)\downarrow)$ of laser radiation probing histological sections decreases (↓). The indicated oncological destruction of the optical anisotropy of the uterine tissue is accompanied by an increase in the probability of the formation of characteristic values $(f_{44} = \pm 1)$ (relations (5), **Table 1**), which characterize the mechanisms of formation of L—states. On the contrary, the probability of the formation of characteristic values $(f_{44} = 0)$ (relations (5), **Table 1**), which characterize the mechanisms of formation of ±C—states, decreases.

These processes quantitatively illustrate the distributions $N(f_{44} = \pm 1)$ and $N(f_{44} = 0)$, which are shown in **Figures 6**, **7**.

The results of the statistical analysis of the distributions $N(f_{44} = 0)$ [fragment (1)] and $M(f_{44} = \pm 1)$ within the representative samplings of histological sections of uterine tumours of all types are presented in **Tables 3**, **4**.

Here are the mean $(\bar{Z}_{i=1;2})$ and standard deviations $(\theta_{i=1;2})$ within all groups of samples $(\bar{Z}_{i=1;2} \pm 2\theta_{i=1;2}2)$ values of the statistical moments of the first and second orders, which characterize the distributions $N(f_{44} = 0)$ (**Table 3**) and $M(f_{44} = \pm 1)$ (**Table 4**).

From the data given in **Table 3** it follows:

statistical moments of the first and second orders, which characterize the distributions $N(f_{44} = 0)$ of the number of characteristic values of Mueller-matrix invariants $f_{44}(m \times n)$ of representative samples of histological sections of myoma biopsy (group 1) and adenocarcinoma of high (group 2) and low (group 3) differentiation, have individual values;

for the statistical moment of the first order, which characterizes the distribution $N(f_{44} = 0)$, a high level of statistical reliability of differentiation of benign and malignant tumours of the uterus—$p_1 < 0.001$and $p_1 < 0.001$, as well as the severity of the oncological condition—$p_{1;2} < 0.001$ is established.

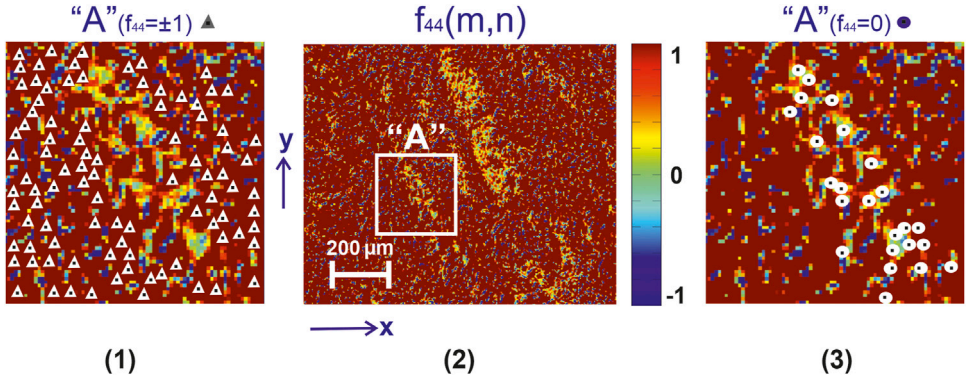

FIGURE 3 | Mueller-matrix image [fragment (2)] of the azimuthal invariant f_{44} $(m \times n)$ of the histological section of myoma biopsy and polarization-singular maps of characteristic values $(f_{44} = \pm 1)$ $(m \times n)$ [fragments (1)]; $(f_{44} = 0)$ $(m \times n)$ [fragments (3)].

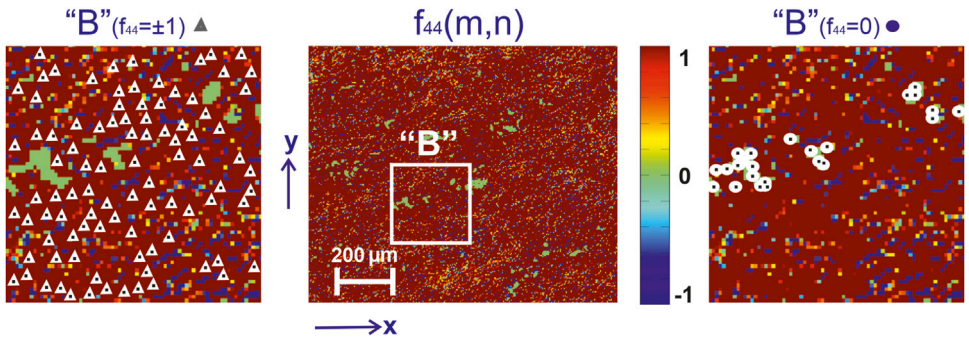

FIGURE 4 | Mueller-matrix image [fragment (2)] of the azimuthal invariant f_{44} $(m \times n)$ of the histological section of biopsy of adenocarcinoma of high differentiation and polarization-singular maps of characteristic values $(f_{44} = \pm 1)$ $(m \times n)$ [fragments (1)]; $(f_{44} = 0)$ $(m \times n)$ [fragments (3)].

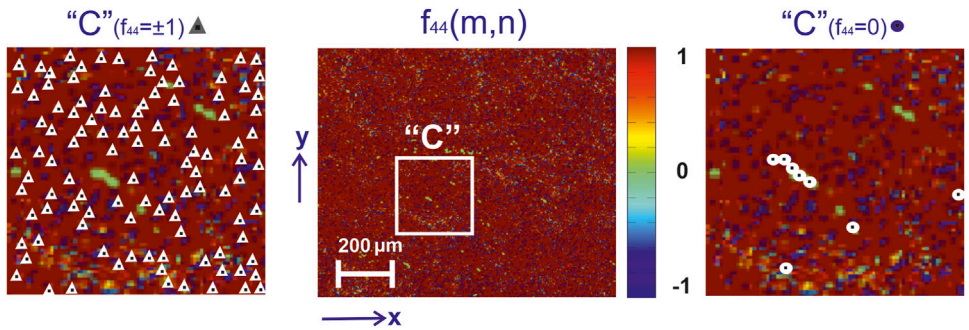

FIGURE 5 | Mueller-matrix image (fragment (2)) of the azimuthal invariant f_{44} $(m \times n)$ of the histological section of biopsy of adenocarcinoma of low differentiation and polarization-singular maps of characteristic values $(f_{44} = \pm 1)$ $(m \times n)$ [fragments (1)]; $(f_{44} = 0)$ $(m \times n)$ [fragments (3)].

statistically significant in differential and intergroup diagnostics are the values for the statistical moment of the second order, which characterizes the distribution $N(f_{44} = 0)$,—$p_1 < 0.05$; $p_2 < 0.05$ and $p_{1;2} < 0.05$.

From the data given in **Table 4** it follows:

- for the statistical moments of the first and second orders, which characterize the average and dispersion of the distributions $N(f_{44} = \pm 1)$ of Mueller-matrix invariants $f_{44}(m \times n)$ of birefringence of the fibrillar networks of the uterine tissue, the statistical reliability of the differentiation of benign and malignant tumours of the uterus was established $p_1 < 0.05$—and $p_2 < 0.05$;

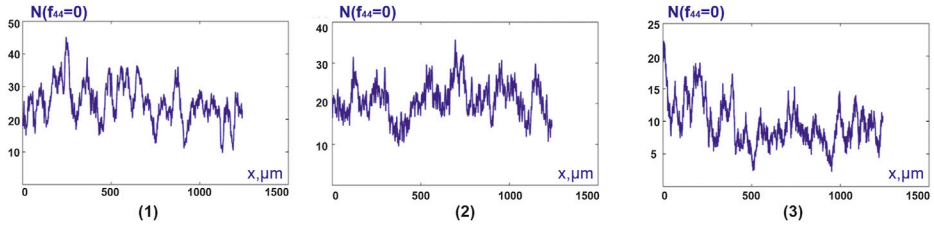

FIGURE 6 | Distributions $N(f_{44} = 0)$ of the number of characteristic values $(f_{44} = 0)$ the Mueller-matrix invariant $f_{44}\,(m \times n)$ of the histological section of myoma [fragment (1)], of adenocarcinoma of high degree of differentiation [fragment (2)] and of low degree of differentiation [fragment (3)] biopsy.

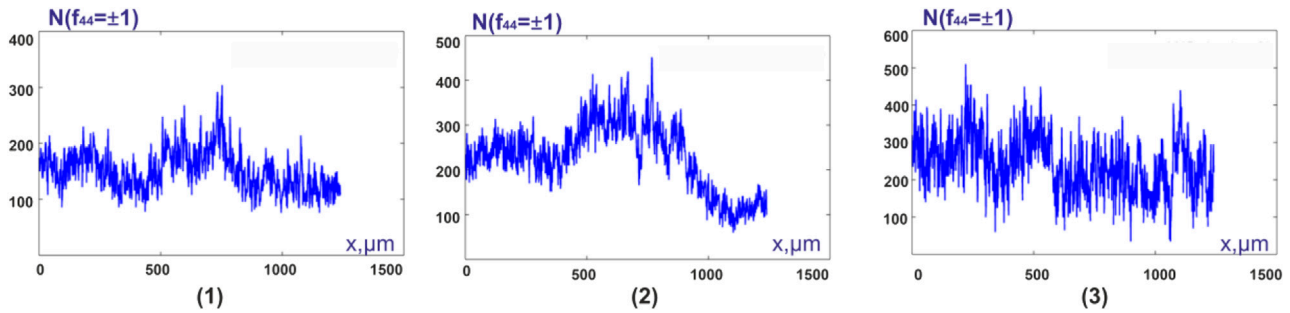

FIGURE 7 | Distributions $M(f_{44} = \pm 1)$ of the number of characteristic values $(f_{44} = \pm 1)$ the Mueller-matrix invariant $f_{44}\,(m \times n)$ of the histological section of myoma [fragment (1)], of adenocarcinoma of high degree of differentiation [fragment (2)] and of low degree of differentiation [fragment (3)] biopsy.

TABLE 3 | Statistical moments of the first and second orders, which characterize the distribution $N(f_{44} = 0)$ of representative samplings of biopsy samples of histological sections of uterine tumours.

Samples	Histological sections of uterus tumours		
Statistical moments	**Group 1 (n = 40)**	**Group 2 (n = 40)**	**Group 3 (n = 40)**
Z_1	0.72±0.031	0.48±0.022	0.23±0.011
$p_1; p_2$	—	$p_1 < 0.001$	$p_2 < 0.001$
$p_{1;2}$	—	$p_{1;2} < 0.001$	
Z_2	0.28±0.012	0.19±0.09	0.11±0.006
$p_1; p_2$	—	$p_1 < 0.05$	$p_2 < 0.05$
$p_{1;2}$	—	$p_{1;2} < 0.05$	

$p_1; p_2$—statistical reliability of differentiation of benign (group 1) and malignant (group 2 + group 3) tumours of the uterus.
$p_{1;2}$—statistical reliability of differentiation of the severity of the oncological process - high (group 2) and low (group 3) differentiated adenocarcinoma.

- ❖ Intergroup diagnostics of samples of histological sections of biopsy of adenocarcinoma with a high and low degree of differentiation turned out to be statistically unreliable,—$p_{1;2} > 0.05$.

CLINICAL APPLICATIONS

With the aim of the possible clinical application of the data of Mueller-matrix mapping of polarization-singular distributions of characteristic values $N(f_{44} = 0)$ and $M(f_{44} = \pm 1)$ we used the principles of evidence-based medicine [47].

To differentiate benign and malignant tumours, for each of the statistical moments $Z_{i=1;2;3;4}$, the sensitivity ($Se_{12} = \frac{a_{12}}{a_{12}+b_{12}}100\%$; $Se_{13} = \frac{a_{13}}{a_{13}+b_{13}}100\%$), specificity ($Sp_{12} = \frac{c_{12}}{c_{12}+d_{12}}100\%$; $Sp_{13} = \frac{c_{13}}{c_{13}+d_{13}}100\%$) and balanced accuracy $[Ac_{12} = 0.5(Sp_{12} + Sp_{12})$; $Ac_{13} = 0.5(Se_{13} + Sp_{13})]$ were calculated. Here, $a_{12}\,(a_{13})$ and $b_{12}\,(b_{13})$ are the number of correct and incorrect diagnoses within group 2 (group 3); and $c_{12}\,(c_{13})$ and $d_{12}\,(d_{13})$ are the same within group 1.

Similarly, to differentiate the grade of cancer, the sensitivity ($Se_{23} = \frac{a_{23}}{a_{23}+b_{23}}100\%$), specificity ($Sp_{23} = \frac{c_{23}}{c_{23}+d_{23}}100\%$) and balanced accuracy ($Ac_{23} = \frac{Se_{23}+Sp_{23}}{2}$ were calculated for each of the statistical moments $Z_{i=1;2;3;4}$. Here, a_{23} and b_{23} the number of correct and incorrect

TABLE 4 | Statistical moments of the first and second orders, which characterize the distribution $M(f_{44} = \pm 1)$ of representative samplings of biopsy samples of histological sections of uterine tumours.

Samples	Histological sections of uterus tumours		
Statistical moments	**Group 1 (n = 40)**	**Group 2 (n = 40)**	**Group 3 (n = 40)**
Z_1	0.41±0.019	0.52±0.024	0.57±0.028
$p_1; p_2$	—	$p_1 < 0.05$	$p_2 < 0.05$
$p_{1;2}$	—	$p_{1;2} > 0.05$	
Z_2	0.18±0.008	0.25±0.012	0.28±0.015
$p_1; p_2$	—	$p_1 < 0.05$	$p_2 < 0.05$
$p_{1;2}$	—	$p_{1;2} > 0.05$	

TABLE 5 | Sensitivity, specificity, balanced accuracy of statistical analysis of distributions of characteristic values $N(f_{44} = 0)$.

Parameters		Group 1		Group 2		Group 3	
Z_1	Se, %	$a_{12} = 1$; $b_{12} = 39$	97.5	$a_{13} = 1$; $b_{13} = 39$	97.5	$a_{23} = 3$; $b_{23} = 37$	92.5
	Sp, %	$c_{12} = 3$; $d_{12} = 37$	92.5	$c_{13} = 2$; $d_{13} = 38$	95	$c_{23} = 4$; $d_{23} = 36$	90
	Ac, %	95		96.25		91.25	
Z_2	Se, %	$a_{12} = 2$; $b_{12} = 38$	95	$a_{13} = 2$; $b_{13} = 38$	95	$a_{23} = 4$; $b_{23} = 36$	90
	Sp, %	$c_{12} = 4$; $d_{12} = 36$	90	$c_{13} = 3$; $d_{13} = 37$	92.5	$c_{23} = 5$; $d_{23} = 35$	87.5
	Ac, %	92.5		93.75		88.75	

TABLE 6 | Sensitivity, specificity, balanced accuracy of statistical analysis of distributions of characteristic values $M(f_{44} = \pm 1)$.

Parameters		Group 1		Group 2		Group 3	
Z_1	Se, %	$a_{12} = 7$; $b_{12} = 33$	82.5	$a_{13} = 6$; $b_{13} = 34$	85	$a_{23} = 13$; $b_{23} = 27$	67.5
	Sp, %	$c_{12} = 9$; $d_{12} = 31$	77.5	$c_{13} = 8$; $d_{13} = 32$	80	$c_{23} = 16$; $d_{23} = 24$	60
	Ac, %	80		82.5		63.75	
Z_2	Se, %	$a_{12} = 9$; $b_{12} = 31$	77.5	$a_{13} = 8$; $b_{13} = 32$	80	$a_{23} = 16$; $b_{23} = 24$	60
	Sp, %	$c_{12} = 12$; $d_{12} = 28$	70	$c_{13} = 10$; $d_{13} = 30$	75	$c_{23} = 18$; $d_{23} = 22$	55
	Ac, %	73.75		77.5		57.5	

diagnoses within group 3; while c_{23} and d_{23} are the same within group 2.

TUMOURS OF THE UTERUS

The results of information analysis using statistical processing of the set of distributions of characteristic values $N(f_{44} = 0)$ and $M(f_{44} = \pm 1)$ within representative samples of histological sections of biopsy of myoma and adenocarcinoma with different degrees of differentiation are presented in **Tables 5**, **6**.

The results shown in **Tables 5**, **6** indicate:

- a high (91.25–96.25%) efficiency of differential diagnosis of uterus tumours by Mueller matrix mapping of histological biopsy sections of myoma and adenocarcinoma with varying degrees of differentiation by statistical analysis of distributions of characteristic values $N(f_{44} = 0)$, —**Table 5**;
- low efficiency (80–82.5%) of statistical analysis of experimental data of polarization-singular Mueller-matrix differentiation of samples of benign and malignant tumours of the uterus;
- unsatisfactory accuracy (57.5–63.75%) of intergroup differentiation based on the data of statistical analysis of distributions of characteristic values $M(f_{44} = \pm 1)$.

TABLE 7 | Optical and geometric parameters of prostate tumour histological sections.

Parameter	Group 1	Group 2	Group 3
Geometric thickness $h, \mu m$	15 ± 0.08	15 ± 0.075	15 ± 0.085
Attenuation (extinction) coefficient τ, cm^{-1}	0.0105 ± 0.0047	0.0107 ± 0.0043	0.0099 ± 0.0048
Depolarization degree $\Lambda, \%$	5 ± 0.14	6 ± 0.16	4 ± 0.13

TABLE 8 | Sensitivity, specificity, balanced accuracy of statistical analysis of distributions of characteristic values $N(f_{44} = 0)$.

Parameters		Group 1		Group 2		Group 3	
Z_1	Se, %	$a_{12} = 3$; $b_{12} = 37$	92.5	$a_{13} = 2$; $b_{13} = 38$	95	$a_{23} = 4$; $b_{23} = 36$	90
	Sp, %	$c_{12} = 4$; $d_{12} = 36$	90	$c_{13} = 3$; $d_{13} = 37$	92.5	$c_{23} = 4$; $d_{23} = 36$	90
	Ac, %	91.25		93.75		90	
Z_2	Se, %	$a_{12} = 4$; $b_{12} = 36$	90	$a_{13} = 3$; $b_{13} = 37$	92.5	$a_{23} = 5$; $b_{23} = 35$	87.5
	Sp, %	$c_{12} = 5$; $d_{12} = 35$	87.5	$c_{13} = 4$; $d_{13} = 36$	90	$c_{23} = 6$; $d_{23} = 34$	85
	Ac, %	88.75		91.25		86.25	

TABLE 9 | Sensitivity, specificity, balanced accuracy of statistical analysis of distributions of characteristic values $M(f_{44} = \pm 1)$.

Parameters		Group 1		Group 2		Group 3	
Z_1	Se, %	$a_{12} = 9$; $b_{12} = 31$	77.5	$a_{13} = 6$; $b_{13} = 34$	85	$a_{23} = 16$; $b_{23} = 24$	60
	Sp, %	$c_{12} = 12$; $d_{12} = 28$	70	$c_{13} = 8$; $d_{13} = 32$	80	$c_{23} = 16$; $d_{23} = 24$	60
	Ac, %	73.75		82.5		60	
Z_2	Se, %	$a_{12} = 11$; $b_{12} = 29$	72.5	$a_{13} = 10$; $b_{13} = 30$	75	$a_{23} = 16$; $b_{23} = 24$	60
	Sp, %	$c_{12} = 12$; $d_{12} = 28$	70	$c_{13} = 11$; $d_{13} = 29$	72.5	$c_{23} = 18$; $d_{23} = 22$	55
	Ac, %	71.25		73.75		57.5	

TUMOURS OF THE PROSTATE

Three Representative Groups of Histological Biopsy Sections of Tumours Were Formed:

- Group 1 consisted of $n = 40$ high differentiated (ISUP 1–3 + 3 on Gleason's pattern scale) adenocarcinoma samples;
- Group 2 consisted of $n = 36$ moderately differentiated (ISUP 2–3—3 + 4; 4 + 3 on Gleason's pattern scale) adenocarcinoma samples;
- Group 3 consisted of $n = 36$ poorly differentiated (ISUP 4–4 + 4; 3 + 5; 5 + 3 on Gleason's Pattern scale) adenocarcinoma samples.

Table 7 presents the optical and geometric parameters of the samples of native histological sections of prostate tumour biopsies from each of the groups.

The results of information analysis using statistical processing of the set of distributions of characteristic values $N(f_{44} = 0)$ and $M(f_{44} = \pm 1)$ within representative samplings of histological sections of prostate adenocarcinoma biopsy with varying degrees of differentiation are presented in **Tables 8**, **9**.

The results shown in **Table 8** indicate a high (90–93.75%) efficiency of differential diagnosis of prostate tumours by Mueller matrix mapping of histological sections of biopsy of adenocarcinoma with varying degrees of differentiation by means of a statistical analysis of distributions $N(f_{44} = 0)$ that determine the mechanisms of formation ±C—states.

The efficiency of differentiation of the degree of statistical analysis of the experimentally obtained distributions of characteristic values $M(f_{44} = \pm 1)$, which determine the mechanisms of formation of—states, turned out to be rather low and did not exceed 60–82.5%, —**Table 9**.

CONCLUSIONS

1) For the first time, the Mueller-matrix approach to the described processes of the formation of polarization-singular states of microscopic images of optically thin histological sections of biopsy of benign and malignant tumours of the uterus and prostate was proposed.
2) The relationship between the characteristic values of the elements of the Mueller matrix and the types of singularity of polarization-inhomogeneous images of optically anisotropic biological preparations of fibroids (uterus) and adenocarcinomas with varying degrees of differentiation (uterus, prostate) has been established.
3) It was found that the statistical analysis of the distributions of the number of characteristic values of the Mueller-matrix invariant, which characterizes the mechanisms of formation $L-$ and $C-$ states of microscopic images of biological preparations is effective for differentiating the polarization properties of such objects associated with pathological changes in the birefringent fibrillar networks of tumours of the uterus and prostate.
4) Within the framework of evidence-based medicine, the sensitivity, specificity and accuracy of the method of azimuthal-invariant mapping of the characteristic values of the Mueller-matrix invariant distributions have been established:
   - ❖ A high (91.25–96.25%) efficiency of differential diagnosis of uterus tumours by Mueller matrix mapping of histological sections of biopsy of myoma and adenocarcinoma with varying degrees of differentiation by statistical analysis of distributions of characteristic values $N(f_{44} = 0)$;
   - ❖ A high (90–93.75%) efficiency of differential diagnosis of prostate tumours by Mueller matrix mapping of histological biopsy sections of adenocarcinoma with varying degrees of differentiation by means of a statistical analysis of distributions $N(f_{44} = 0)$ that determine the mechanisms of formation ±C—states.

DATA AVAILABILITY STATEMENT

The original contributions presented in the study are included in the article/Supplementary Material, further inquiries can be directed to the corresponding author.

ETHICS STATEMENT

The studies involving human participants were reviewed and approved by the Ethical approval was obtained from the Ethics Committee of the Bureau of Forensic Medicine of the Chernivtsi National University and the Bukovinian State Medical University (Chernivtsi, Ukraine), and written informed consent was obtained from all subjects prior to study initiation. The patients/participants provided their written informed consent to participate in this study.

AUTHOR CONTRIBUTIONS

Manuscript preparation: AU, VU, and LT. Measurements, data processing: AS, IS, YU, YT, AD, VG and PG.

FUNDING

This work received funding from National Research Foundation of Ukraine, Project 2020.02/0061.

REFERENCES

1. Freund I, Soskin MS, and Mokhun AI. Elliptic Critical Points in Paraxial Optical fields. *Opt Commun* (2002) 208:223–53. doi:10.1016/s0030-4018(02)01585-7
2. Soskin MS, Denisenko V, and Freund I. Optical Polarization Singularities and Elliptic Stationary Points. *Opt Lett* (2003) 28:1475–7. doi:10.1364/ol.28.001475
3. Dennis MR. Polarization Singularities in Paraxial Vector fields: Morphology and Statistics. *Opt Commun* (2002) 213:201–21. doi:10.1016/s0030-4018(02)02088-6
4. Nye JF. Lines of Circular Polarization in Electromagnetic Wave fields. *Proc R Soc Lond A* (1983) 389:279–90. doi:10.1098/rspa.1983.0109
5. Flossmann F, Schwarz UT, Maier M, and Dennis MR. Polarization Singularities from Unfolding an Optical Vortex through a Birefringent crystal. *Phys Rev Lett* (2005) 95:253901. doi:10.1103/physrevlett.95.253901
6. Flossmann F, Schwarz UT, Maier M, and Dennis MR. Stokes Parameters in the Unfolding of an Optical Vortex through a Birefringent crystal. *Opt Express* (2006) 14:11402–11. doi:10.1364/oe.14.011402
7. Angelsky O, Besaha R, Mokhun A, Mokhun I, Sopin M, and Soskin M. Vasnetsov M Singularities in Vectoral fields *SPIE. Proc* (1999) 3904:40–55. doi:10.1117/12.370443
8. Freund I, Mokhun AI, Soskin MS, Angelsky OV, and Mokhun II. Stokes Singularity Relations. *Opt Lett* (2002) 27(7):545–7. doi:10.1364/ol.27.000545
9. Berry MV, and Dennis MR. Polarization Singularities in Isotropic Random Vector Waves. *Proc R Soc Lond A* (2001) 457:141–55. doi:10.1098/rspa.2000.0660
10. Bickel WS, and Bailey WM. Stokes Vectors, Mueller Matrices, and Polarized Scattered Light. *Am J Phys* (1985) 53:468–78. doi:10.1119/1.14202
11. Lu S-Y, and Chipman RA. Interpretation of Mueller Matrices Based on Polar Decomposition. *J Opt Soc Am A* (1996) 13:1106–13. doi:10.1364/josaa.13.001106
12. Ghosh N, Wood M, and Vitkin A. Polarized Light Assessment of Complex Turbid Media Such as Biological Tissues Using Mueller Matrix Decomposition. *Science* (2010) 9:253–82. doi:10.1201/9781439806296-c9
13. Gil JJ. Characteristic Properties of Mueller Matrices. *J Opt Soc Am A* (2000) 17:328–34. doi:10.1364/josaa.17.000328
14. Angelsky O, Ushenko A, Ushenko Y, Pishak V, and Peresunko A. Correlation and Topological Approaches in Diagnostics of the Structure and Physiological State of Birefringent Biological Tissues. in: *Handbook Of Photonics For Biomedical Science* (2010). p. 283–322. doi:10.1201/9781439806296-c10
15. Ushenko YA, Boychuk TM, Bachynsky VT, and Mincer OP. *Diagnostics of Structure and Physiological State of Birefringent Biological Tissues: Statistical, Correlation and Topological Approaches* Handbook Of Coherent-Domain Optical Methods (2013), New York, NY: Springer. p. 107–48. doi:10.1007/978-1-4614-5176-1_3
16. Ghosh N. Tissue Polarimetry: Concepts, Challenges, Applications, and Outlook. *J Biomed Opt* (2011) 16:110801. doi:10.1117/1.3652896

17. Jacques SL, Boas D, and Pitris C. *Ramanujam N Polarized Light Imaging of Biological Tissues* Handbook Of Biomedical Optics. Boca Raton, London, New York: CRC Press (2011). 649–69.
18. Vitkin A, Ghosh N, and Martino Ad.. *Tissue Polarimetry in Photonics: Scientific Foundations, Technology And Applications*. in: DL Andrews, editor, IV. Hoboken, New Jersey: John Wiley & Sons (2015). 239–321. doi:10.1002/9781119011804.ch7
19. Tuchin VV. Tissue Optics and Photonics: Light-Tissue Interaction. *Jbpe* (2015) 1:98–134. doi:10.18287/jbpe-2015-1-2-98
20. Tuchin VV. *Tissue Optics: Light Scattering Methods and Instruments for Medical Diagnosis*. 3rd ed. Bellingham, WA: Society of Photo-Optical Instrumentation Engineers SPIE Press (2015). doi:10.1117/3.1003040
21. Swami MK, Patel HS, and Gupta PK. Conversion of 3×3 Mueller Matrix to 4×4 Mueller Matrix for Non-depolarizing Samples. *Opt Commun* (2013) 286: 18–22. doi:10.1016/j.optcom.2012.08.094
22. Izotova VF, Maksimova IL, Nefedov IS, and Romanov SV. Investigation of Mueller Matrices of Anisotropic Nonhomogeneous Layers in Application to an Optical Model of the Cornea. *Appl Opt* (1997) 36:164. doi:10.1364/ao.36.000164
23. Manhas S, Swami MK, Buddhiwant P, Ghosh N, Gupta PK, and Singh J. Mueller Matrix Approach for Determination of Optical Rotation in Chiral Turbid media in Backscattering Geometry. *Opt Express* (2006) 14:190. doi:10.1364/opex.14.000190
24. Deng Y, Zeng S, Lu Q, Zhu D, and Luo Q. Characterization of Backscattering Mueller Matrix Patterns of Highly Scattering media with Triple Scattering assumption. *Opt Express* (2007) 15:9672. doi:10.1364/oe.15.009672
25. Lu S-Y, and Chipman RA. Interpretation of Mueller Matrices Based on Polar Decomposition. *J Opt Soc Am AA* (1996) 13:1106. doi:10.1364/josaa.13.001106
26. Guo Y, Zeng N, He H, Yun T, Du E, and Liao RA Study on Forward Scattering Mueller Matrix Decomposition in Anisotropic Medium. *Opt Express* (2013) 21:18361. doi:10.1364/oe.21.018361
27. Borovkova M, Peyvasteh M, Dubolazov O, Ushenko Y, Ushenko V, Bykov A, et al.Complementary Analysis of Mueller-Matrix Images of Optically Anisotropic Highly Scattering Biological Tissues. *J Eur Opt Soc.-Rapid Publ* (2018) 14(1):20. doi:10.1186/s41476-018-0085-9
28. Ushenko V, Sdobnov A, Syvokorovskaya A, Dubolazov A, Vanchulyak O, Ushenko A, et al.3D Mueller-Matrix Diffusive Tomography of Polycrystalline Blood Films for Cancer Diagnosis. *Photonics* (2018) 5(4):54. doi:10.3390/photonics5040054
29. Ushenko A, Sdobnov A, Dubolazov A, Grytsiuk M, Ushenko Y, and Bykov A. Meglinski I Stokes-Correlometry Analysis of Biological Tissues with Polycrystalline Structure. *IEEE J Selected Top Quan Electro* (2019) 25(1): 8438957. doi:10.1109/jstqe.2018.2865443
30. Trifonyuk L, Baranowski W, Ushenko V, Olar O, Dubolazov A, Ushenko Y, et al.2D-Mueller-matrix Tomography of Optically Anisotropic Polycrystalline Networks of Biological Tissues Histological Sections. *Opto-electronics Rev* (2018) 26(3):252–9. doi:10.1016/j.opelre.2018.07.001
31. Trifonyuk L, Sdobnov A, Baranowski W, Ushenko V, Olar O, Dubolazov A, et al.Differential Mueller Matrix Imaging of Partially Depolarizing Optically Anisotropic Biological Tissues. *Lasers Med Sci* (2020) 35(4):877–91. doi:10.1007/s10103-019-02878-2
32. Borovkova M, Trifonyuk L, Ushenko V, Dubolazov O, Vanchulyak O, Bodnar G, et al.Mueller-matrix-based Polarization Imaging and Quantitative Assessment of Optically Anisotropic Polycrystalline Networks. *PLoS ONE* (2019) 14(5):e0214494. doi:10.1371/journal.pone.0214494
33. Wang LV, and Wu H-I. *Biomedical Optics: Principles and Imaging*. John Wiley & Sons (2009). doi:10.1002/9780470177013
34. Ushenko VA, Hogan BT, Dubolazov A, Grechina AV, Boronikhina TV, Gorsky M, et al.Embossed Topographic Depolarisation Maps of Biological Tissues with Different Morphological Structures. *Sci Rep* (2021) 11(1):3871. doi:10.1038/s41598-021-83017-2
35. Angelsky OV, Ushenko AG, Ushenko YA, and Ushenko YG. Polarization Singularities of the Object Field of Skin Surface. *J Phys D: Appl Phys* (2006) 39: 3547–58. doi:10.1088/0022-3727/39/16/005
36. Angelsky Ov Ushenko AG, and Angelska AO. Ushenko YuA Correlation- and Singular-Optical Approaches in Diagnostics of Polarization Inhomogeneity of Coherent Optical fields from Biological Tissues *Ukr. J Phys Opt* (2007) 8(2): 105–23. doi:10.3116/16091833/8/2/106/2007
37. Ushenko VO, Trifonyuk L, Ushenko YA, Dubolazov OV, Gorsky MP, and Ushenko AG. Polarization Singularity Analysis of Mueller-Matrix Invariants of Optical Anisotropy of Biological Tissues Samples in Cancer Diagnostics. *J Opt* (2021) 23(6):064004. doi:10.1088/2040-8986/abf97a
38. Mohler J. *Prostate Cancer J Natl Compr Cancer Netw* (2010) 8:162–200. doi:10.6004/jnccn.2010.0010
39. Grönberg H. *Prostate Cancer Epidemiol Lancet* (2003) 361:859–64.
40. Ilic D, Neuberger MM, Djulbegovic M, and Dahm P. *Screening for Prostate Cancer* Cochrane Database Of Systematic Reviews (2013).
41. Albertsen PC, and Hanley JA. 20-Year Outcomes Following Conservative Management of Clinically Localized Prostate Cancer. *Jama* (2005) 293: 2095–101. doi:10.1001/jama.293.17.2095
42. Sung H, Ferlay J, Siegel RL, Laversanne M, Soerjomataram I, Jemal A, et al.Global Cancer Statistics 2020: GLOBOCAN Estimates of Incidence and Mortality Worldwide for 36 Cancers in 185 Countries. *CA A Cancer J Clin* (2021) 71:209–49. doi:10.3322/caac.21660
43. Garcia-Lopez P, Garcia-Marin V, and Freire MThe Histological Slides and Drawings of Cajal. *Front Neuroanat* (2010) 4:9. doi:10.3389/neuro.05.009.2010
44. Marchesini R, Bertoni A, Andreola S, Melloni E, and Sichirollo AE. Extinction and Absorption Coefficients and Scattering Phase Functions of Human Tissues *In Vitro*. *Appl Opt* (1984) 28:2318–24. doi:10.1364/AO.28.002318
45. Edwards DK, Gier JT, Nelson KE, and Roddick RD. Integrating Sphere for Imperfectly Diffuse Samples*. *J Opt Soc Am* (1961) 51:1279–88. doi:10.1364/josa.51.001279
46. Goodman JW. *Statistical Properties of Laser Speckle Patterns*. Berlin, Heidelberg: Springer (1975). p. 9–75. doi:10.1007/978-3-662-43205-1_2
47. Robinson SP. *Principles of Forensic Medicine Greenwich Medical Media* (1996).

Conflict of Interest: The authors declare that the research was conducted in the absence of any commercial or financial relationships that could be construed as a potential conflict of interest.